UNDERCOOLING AND CONTACT RESISTANCE IN STAGNATION-FLOW SOLIDIFICATION ON A SEMI-INFINITE SUBSTRATE

R. H. Rangel[1] and X. Bian

Department of Mechanical and Aerospace Engineering
University of California, Irvine
Irvine, CA 92697 USA

Phone: (714) 824-4033, Fax: (714) 824-8585, e-mail: rhrangel@uci.edu

Abstract

The inviscid stagnation-flow solidification problem is studied numerically including the effect of contact resistance and undercooling during solidification. The effect of contact resistance at the initial liquid-solid contact plane is demonstrated by comparing the solidification behavior for cases with different contact heat transfer coefficient. The effect of undercooling is examined by comparing model predictions including this effect with those obtained when equilibrium solidification with interface temperature at the thermodynamic equilibrium temperature is used. The study shows that undercooling delays the start of solidification but has a negligible effect on the long time behavior of the process. A sufficiently large contact resistance may prevent solidification when undercooling is included in the model.

Submitted to

International Journal of Heat and Mass Transfer

First submission: June 25, 1997

Revised: Sept. 23, 1997

[1]Author to whom correspondence should be addressed.

Nomenclature

A	potential-flow strain rate
a_α	α_ℓ/α_s, ratio of the liquid to solid thermal diffusivity
a_k	k_ℓ/k_s, ratio of the liquid to solid thermal conductivity
c	solid-phase specific heat
Ev	activation energy
h	substrate/deposit heat transfer coefficient
h_{sf}	latent heat of solidification
k	thermal conductivity
K	kinetics coefficient for undercooling solidification
R	universal gas constant
s	solid front position
$\dot{s}$	solid front velocity ($\dot{s} = ds/dt$)
$\tilde{s}$	dimensionless solid front position ($\tilde{s} = s\sqrt{\frac{A}{\alpha_s}}$)
St	Stefan number ($c(T_m - T_0)/h_{sf}$)
T	temperature
t	time

u velocity component parallel to the solid front

v velocity component normal to the solid front

y spatial coordinate normal to the solid front

$\tilde{y}$ dimensionless spatial coordinate normal to the substrate ($\tilde{y} = y/\sqrt{\alpha_s/A}$)

Y normal coordinate measured from the solid front ($Y = y - s(t)$)

Greek symbols

α thermal diffusivity

η transformed coordinate

θ nondimensional temperature $[(T - T_m)/(T_m - T_0)]$

τ nondimensional time ($\tau = At$)

Subscripts

d deposit

i initial

in interface

ℓ liquid phase

m equilibrium melting point

n nucleation

s solid phase, substrate

Diacritical mark

$\sim$ nondimensional

1. Introduction

In many solidification processes such as casting and spray deposition, the motion of the liquid phase plays an important role in modifying the rates of solidification [1]-[11]. Due to the complexity of these processes, several theoretical studies have uncoupled the fluid mechanics from the heat transfer and solidification mechanisms to make the problem more tractable. The stagnation-flow solidification models presented by Rangel and Bian [7]-[9] demonstrate the effect of the fluid motion on the solidification behavior of the molten metal.

The quality of thermal contact between the substrate and the impinging flow of molten metal plays an important role in the solidification process. Experimental and numerical

studies of the thermal conductance between the substrate and the melt can be found in the work of Wang and Matthys [4][17][18]. Large scales of undercooling may exist in the case of rapid solidification. Under these conditions, the interface is not in thermodynamic equilibrium and the interface velocity is governed by the kinetic effects in addition to the rate of external heat extraction [18]. In the work of Wang and Matthys [18] and Kang *et al*[3][20], the mechanism of undercooling during rapid solidification has been studied by applying a simplified undercooling relationship.

In the present work, the above mentioned stagnation-flow solidification model is enhanced by including a finite thermal contact resistance between the substrate and the stagnation flow of the melt. The mechanism of crystal growth kinetics governed undercooling solidification [22] has also been included in the model to replace the classical assumption that the solidification front is at the thermodynamic equilibrium phase temperature. Analytical and numerical solutions of the stagnation-flow solidification problem have been presented by Rangel and Bian for inviscid [7] [8] and viscous flows [9] for a constant-temperature substrate. Later Bian and Rangel extended the inviscid model to include the effect of a finite-thickness substrate [10]. For the case of metal flows, the inviscid-flow assumption is appropriate since the thermal boundary layer is much thicker than the viscous one [9]. Here we extend these previous models to consider the case of a very thick substrate including the

effects of undercooling during solidification and contact resistance at the contact plane.

2. Mathematical Formulation

The governing equations for this problem are described in [7]. The heat conduction equation for the solid substrate is,

$$\frac{\partial T_s}{\partial t} = \alpha_s \frac{\partial^2 T_s}{\partial y^2} \qquad \text{in } -\infty < y < 0,\ t > 0 \tag{1}$$

with the boundary condition: $T_s(y,t) \to T_0$ as $y \to -\infty$.

Assuming inviscid flow [9], the thermal energy equation of the liquid is

$$\frac{\partial T_\ell}{\partial t} - 2A[y - s(t)]\frac{\partial T_\ell}{\partial y} = \alpha_\ell \frac{\partial^2 T_\ell}{\partial y^2} \qquad \text{in } 0 < y < \infty,\ t > 0 \tag{2}$$

with the boundary condition: $T_\ell(y,t) \to T_i$ as $y \to \infty$.

The thermal contact between the stagnation flow and the substrate at the initial contact plane is taken into account by introducing a heat transfer coefficient [21]

$$h = q''/(T_d - T_s)|_{y=0} \tag{3}$$

where q'' is the heat flux and $(T_d - T_s)|_{y=0}$ is the temperature jump at the contact plane.

Hence, the boundary condition for the heat transfer between the deposit and the substrate is

$$-k_d\frac{\partial T}{\partial y} = -k_s\frac{\partial T}{\partial y} = h(T_d - T_s) \qquad \text{at } y = 0 \tag{4}$$

Here $k_d = k_\ell$ before solidification starts and $k_d = k_s$ after solidification occurs, where we assume that the solidified deposit has the same properties as the substrate. The solid-liquid interface energy-balance equation

$$\rho h_{sf}\frac{ds}{dt} = k_s\frac{\partial T_s}{\partial y} - k_\ell\frac{\partial T_\ell}{\partial y} \qquad \text{at } y = s(t) \tag{5}$$

is coupled with the solidification rate relation with undercooling [23]

$$\frac{ds}{dt} = K_m(T_m - T_{in}) \tag{6}$$

where K_m is the kinetics coefficient, T_{in} is the solidification interface temperature with undercooling. The above relation is a linear approximation to the crystal growth model for a pure melt [22]

$$\frac{ds}{dt} = V_0 \exp\left[-\frac{E_v}{RT_m}\frac{\Delta T_{in}}{T_{in}}\right]\left[1 - \exp\left[-\frac{h_{sf}}{RT_m}\frac{\Delta T_{in}}{T_{in}}\right]\right] \tag{7}$$

where V_0 is a molecular attachment velocity, E_v is an activation energy, R is the universal gas constant.

The onset of solidification corresponds to the time when the temperature of the melt at the plane of contact with the solid substrate decreases to the nucleation temperature T_n. The thermal energy equation of the solidified deposit is the same as equation (1) except that if the melt material is different from the substrate, the value of α_s will be different. The solution domain for the solidified region is $0^+ < y < s(t)$. While the solution domain for the melt is $s(t) < y < \infty$.

3. Long-time behavior

The existence of a semi-infinite substrate brings about an interesting analytical solution valid for very long times and for the case when the substrate and deposit are of the same material. This will be contrasted below with the long time solutions for the case of solidification or remelting of semi-infinite media without fluid flow (the Stefan solidification problem [24]) and the stagnation-flow solidification on a finite thickness substrate [7].

The solution of eqs. (1), (2) and (5) valid as $t \to \infty$ may be obtained by postulating that the problem is steady in a reference frame moving with the phase interface front and that the velocity of this front $\dot{s}$ is a constant. As will be shown below $\dot{s}$ is actually a negative

constant. To this end, let $Y = y - s(t)$ so that eqs. (1) and (2) become (after dropping the transient terms):

$$\alpha_s \frac{\partial^2 T_s}{\partial Y^2} + \dot{s}\frac{\partial T_s}{\partial Y} = 0 \tag{8}$$

$$\alpha_\ell \frac{\partial^2 T_\ell}{\partial Y^2} + (\dot{s} + AY)\frac{\partial T_\ell}{\partial Y} = 0 \tag{9}$$

subject to the same boundary conditions described in the context of eqs. (1) and (2). The solutions of eqs. (8) and (9) are obtained as:

$$\frac{T_s - T_m}{T_m - T_o} = -1 + \exp\left(-\frac{\dot{s}}{\alpha_s}Y\right), \qquad Y \leq 0 \tag{10}$$

$$\frac{T_\ell - T_m}{T_i - T_m} = \frac{\operatorname{erf}\left[\sqrt{\frac{A}{2\alpha_\ell}}\left(Y - \frac{\dot{s}}{A}\right)\right] - \operatorname{erf}\left(\frac{\dot{s}}{\sqrt{2\alpha_\ell A}}\right)}{1 - \operatorname{erf}\left(\frac{\dot{s}}{\sqrt{2\alpha_\ell A}}\right)}, \qquad Y \geq 0 \tag{11}$$

The front velocity is obtained from the energy balance at the phase interface, eq. (5) which yields:

$$\dot{\tilde{s}}\left(1 + \frac{1}{St}\right) = -\sqrt{\frac{2}{\pi}}\frac{a_k}{\sqrt{a_\alpha}}\theta_i \frac{\exp\left(-\frac{\dot{\tilde{s}}^2}{2a_\alpha}\right)}{1 - \operatorname{erf}\left(\frac{\dot{\tilde{s}}}{\sqrt{2a_\alpha}}\right)} \tag{12}$$

This is a nonlinear algebraic equation from which the long-time front velocity can be obtained. It is worth nothing that for all positive values of θ_i and St (liquid above melting point and solid below melting point), the front velocity is negative implying that the only long-time solution is the one with remelting.

Figure 1 shows the solution of eq. (12) for typical values of θ_i and St. This solution should be contrasted with the one for the Stefan solidification problem [24] without liquid motion. In that case, both solidification and melting solutions are possible depending on the initial conditions and the front advances with a velocity proportional to $\sqrt{t}$. On the other hand, in the stagnation-flow solidification on a finite-thickness substrate (including the case of zero initial thickness), the front asymptotes to a fixed value as $t \to \infty$ [7]-[10].

4. Finite-difference solution

In order to facilitate the numerical solution, the set of equations (1)-(2) are transformed to dimensionless form,

$$\frac{\partial \theta_s}{\partial \tau} = \frac{\partial^2 \theta_s}{\partial \tilde{y}^2} \qquad \text{in} \quad -\infty < \tilde{y} < 0 \quad \text{and } 0 < \tilde{y} < \tilde{s} \tag{13}$$

$$\frac{\partial \theta_\ell}{\partial \tau} - 2[\tilde{y} - s(\tilde{t})]\frac{\partial \theta_\ell}{\partial \tilde{y}} = a_\alpha \frac{\partial^2 \theta_\ell}{\partial \tilde{y}^2} \qquad \text{in} \quad \tilde{s} < \tilde{y} < \infty \tag{14}$$

The boundary condition at the initial substrate surface [Eq. (4)] is nondimensionalized to

$$\theta_d - \theta_s = \tilde{k}_s \frac{\partial \theta_s}{\partial \tilde{y}} = \tilde{k}_d \frac{\partial \theta_d}{\partial \tilde{y}} \qquad \text{at} \quad \tilde{y} = 0 \tag{15}$$

where

$$\tilde{k}_s = \frac{k_s}{h\sqrt{\alpha_s/A}} \qquad \text{and} \qquad \tilde{k}_d = \frac{k_d}{h\sqrt{\alpha_s/A}} \tag{16}$$

The energy-balance equation at the solidification front [Eq. (5)] is transformed to

$$\frac{1}{St}\frac{d\tilde{s}}{d\tau} = \frac{\partial\theta_s}{\partial\tilde{y}} - a_k\frac{\partial\theta_\ell}{\partial\tilde{y}} \tag{17}$$

while the undercooling relation [Eq. (6)] becomes

$$\frac{d\tilde{s}}{d\tau} = -\tilde{K}_m\theta_{in} \tag{18}$$

where

$$\tilde{K}_m = \frac{1}{\sqrt{\alpha_s A}}(T_m - T_0)K_m \tag{19}$$

Note that θ_{in} is a negative number. The solution domain consists of three regions, namely the substrate, the solidified deposit, and the liquid flow. The following transformations render these regions finite and also reduce the problem to a fixed boundary problem. The relation

$$\eta_s = \frac{2}{\pi}\tan^{-1}(\tilde{y}) \tag{20}$$

is employed in the substrate to transform the solution domain ($-\infty < \tilde{y} < 0$) to ($-1 < \eta_s < 0$). For the liquid region, the relation

$$\eta_\ell = \frac{2}{\pi}\tan^{-1}(\tilde{y} - \tilde{s}) \tag{21}$$

transforms the solution domain ($\tilde{s} < \tilde{y} < \infty$) to ($0 < \eta_\ell < 1$). Before the onset of solidification, the substrate energy equation (13), the liquid energy equation (14) as well as the energy equation governing the heat transfer between the deposit and the substrate (15) are solved numerically by using the Thomas algorithm [25] in the transformed domains after rewriting the transformed equations into finite-difference form using the Crank-Nicolson scheme [25].

During solidification, the region in contact with the substrate (the solidified deposit) must be included in the solution. In addition to the above-mentioned substrate and liquid phase energy equations, the solid-phase energy equation of the solidified deposit is solved after a transformation introduced as

$$\eta_d = \frac{\tilde{y}}{\tilde{s}} \tag{22}$$

The transformed equation for the solidified deposit is solved in the same way as the transformed equation for the other two regions. Since Eq. (22) is singular at the onset of solidification, the initial solid thickness $\tilde{s}$ is obtained from Eq. (18) with a simple Euler integration.

Once this small but finite thickness is obtained, the transformation given by Eq. (22) maybe used in the solidified deposit. The solid front is tracked by solving the transformed version of Eq. (17) after the temperature distributions are obtained at each time step coupled with Eq. (18) from which the interface temperature is determined. At the substrate/deposit contact plane, the substrate temperature, T_s, and the deposit temperature, T_d, are obtained from the transformed form of Eq. (15). In transforming the deposit side of equation (15), Eq. (20) is used before solidification starts while Eq. (22) is used after the onset of solidification.

5. Results and discussion

In this section, numerical results for the case of liquid aluminum flowing onto a substrate of the same material are presented. For all the calculations, the initial liquid temperature is 100K above its melting temperature ($933K$), while the initial substrate temperature is 300K. The strain rate is $10^4 s^{-1}$ which is typical in high-speed spray deposition processes. Experimental measurements [18]-[20] show that the value of undercooling ($T_{in} - T_m$) is approximately 40 to 50K. In the current calculations, the undercooling is set at 50K for the reference cases. The kinetics coefficient is chosen as $0.05 m s^{-1} K^{-1}$ [18]. Parametric studies showing the effect of the undercooling and the kinetic coefficient are presented as well. For all the calculations, the dimensionless time step is equal to 10^{-4}. The number of grid points

for each region (the solid substrate, the solidified liquid region and the liquid region) is set to 400. Numerical tests indicate that this provides appropriate numerical accuracy.

Figure 2 shows the nondimensional time evolution of the solid front location. Initially, the solid front advances into the solidifying liquid. Eventually, the solid-front reaches a maximum and remelting of the solidified deposit occurs. This is the result of the continued convective heat flux from the liquid in the presence of very thick substrate. The remelting process continues until all the solidified deposit is remelted, at which point the calculation is terminated. Beyond this point, remelting of the substrate would occur. The long-time behavior is that described earlier, with the melting front advancing into the substrate with a constant velocity.

It may also be observed in Fig. 2(a) that as the heat transfer coefficient h_c decreases, the increasing contact resistance delays the onset of solidification and reduces the maximum solidified thickness. In addition, the time to completely remelt the solid deposit is reduced.

The difference in the solidification behavior between the model that takes into account the mechanism of undercooling (thin curves) and the one that assumes that solidification occurs at the thermodynamic equilibrium temperature (thick curves) may be observed in Fig. 2(b). The main effect of undercooling is a delay in the onset of solidification for typical values of the interface contact resistance. Moreover, with a sufficiently high contact resistance

($h_c = 10^5 Wm^{-2}K^{-1}$ in this case), no solidification is observed when undercooling is taken into account. It is important to note, however, that the long-time behavior of the solid front evolution is independent of the effect of undercooling. For sufficiently long times, the solid front temperature approaches the thermodynamic equilibrium phase change temperature.

Figure 3 shows the dimensionless time evolution of the contact-plane temperatures. The contact-plane temperature of the deposit is shown in Fig. 3(a), that of the substrate is shown in Fig. 3(b), while their difference (the temperature jump across the contact resistance) is shown in Fig. 3(c). Before the onset of solidification, the temperature of the liquid at the substrate/deposit contact interface decreases due to heat transfer from the liquid to the solid substrate. After solidification begins, there is a significant increase of the temperature of the deposit at the contact interface due to the release of the latent heat of solidification. After this event, the temperature of the now-solid deposit at the substrate/deposit interface will continue to decrease for a while but will eventually increase as the solid front reaches a maximum height and remelting occurs. The abrupt increase of the deposit temperature at the substrate-deposit interface at the onset of solidification is caused by the relatively high solidification velocity resulting from the large initial undercooling and the associated release of the latent heat. As expected, when undercooling is neglected, solidification begins when the deposit temperature reaches the thermodynamic-equilibrium phase-change tem-

perature. For increasing contact resistance, the onset of solidification is delayed further. Figure 3(b) demonstrates that the substrate temperature at the substrate-deposit contact plane monotonically increases with time and furthermore, it is fairly insensitive to the onset of solidification. The temperature jump across the contact resistance, Fig. 3(c), decreases as the heat flux toward the substrate decreases.

Figure 4 shows the time variation of the phase interface temperature (the solid-front temperature). This front does not exist before the onset of solidification. It can be observed in this figure that the temperature of the solidification front increases very rapidly after the onset of solidification from the nucleation temperature to a temperature below the thermodynamic equilibrium temperature. As time increases, the phase interface temperature gradually approaches the thermodynamic equilibrium phase-change temperature. As the contact resistance increases (lower value of h), the onset of solidification is delayed but the solid front temperature approaches the thermodynamic-equilibrium temperature sooner.

The effect of undercooling may be further assessed with the help of Fig. 5. This figure shows the temperature distributions at different times for the case of $h = 10^6 Wm^{-2}K^{-1}$ with undercooling (a) and at thermodynamic equilibrium (b). Fig. 5(a) illustrates the formation of a temperature cusp at the solidification front ($\tilde{y} = 0$) at the onset of solidification ($\tau = 0.189$). On the other hand, in Fig. 5(b), there is no local maximum in the temperature

distribution before or after solidification starts since no undercooling mechanism is taken into account. The temperature cusp in the first case is due to the faster heat release resulting from solidification at the lower (undercooling) temperature. This rate of heat release is initially faster than the heat diffusion mechanism.

The effect of the degree of initial undercooling can be observed in Fig. 6 which shows the time evolution of the location and temperature of the phase interface. It can be seen that a larger initial undercooling temperature delays the onset of solidification but yields a higher initial solidification rate. However these effects are minimal over a typical range of undercooling levels.

5. Conclusions

A numerical solution of the stagnation-flow solidification problem of a metal on a semi-infinite substrate, including the effect of undercooling and contact resistance has been developed by means of finite differences.

The solidification rate is initially governed by the mechanism of crystal growth kinetics. As the solid-front approaches the thermodynamic equilibrium phase-change temperature, the rate of solidification is governed by the thermodynamic equilibrium energy balance at the interface. Because of the continued influx of thermal energy from the flowing melt and

the semi-infinite character of the substrate, the long-term solution involves remelting of the substrate.

It is also shown that undercooling delays the onset of solidification, especially for a larger contact resistance. If the substrate/deposit contact resistance is large enough, no solidification is observed when undercooling is included in the model.

An analytical solution for the long-time behavior of the process indicates that remelting of the substrate will proceed at a constant velocity.

Acknowledgement

This work has been supported by a grant from the National Science Foundation (DMI 95-28684) and a collaborative UC/Los Alamos Research (CULAR) grant.

References

[1] C. H. Amon, K. S. Schmaltz, R. Merz, and F. B. Prinz, Numerical and Experimental Investigation of Interface Bonding Via Substrate Remelting of an Impinging Molten Metal Droplet, *Trans. of ASME,* **118**, 164-172 (1996).

[2] H. Liu, E. J. Lavernia and R. H. Rangel, Numerical Simulation of Substrate Impact and Freezing of Droplets in Plasma Spray Processes, *J. Phys. D: Appl. Phys.* **26**, 1900-1908

(1993).

[3] B. Kang, Z. Zhao, and D. Poulikakos, Solidification of Liquid Metal Droplets Impacting Sequentially on a Solid Surface, *Transactions of the ASME,* **116**, 436-444 (1994).

[4] G. X. Wang and E. F. Matthys, Experimental Investigation of Interfacial Conductance for Molten Metal Solidification on a Substrate, *J. Heat Transfer,* **118**, 157-163 (1996).

[5] J.-P. Delplanque and R. H. Rangel, An Improved Model for Droplet Solidification on a Flat Surface, *J. Material Sc.*, in press (1997).

[6] J. P. Delplanque, E. J. Lavernia and R. H. Rangel, Multidirectional Solidification Model for the Description of Micropore Formation in Spray Deposition Processes, *Numerical Heat Transfer Part A-Applications,* **30**, 1-18 (1996).

[7] R. H. Rangel and X. Bian, The Inviscid Stagnation-flow Solidification Problem, *Int. J. Heat Mass Transfer*, **39**, 1591-1602 (1996).

[8] R. H. Rangel and X. Bian, Numerical Solution of the Inviscid Stagnation-Flow Solidification Problem, *Numerical Heat Transfer-Part A*, **28**, 589-603 (1995).

[9] X. Bian and R. H. Rangel, The Viscous Stagnation-Flow Solidification Problem, *Int. J. Heat Mass Transfer*, **39**, 3581-3594 (1996).

[10] X. Bian and R. H. Rangel, Stagnation-Flow Solidification on a Finite Thickness Substrate, *Int. J. Heat Mass Transfer*, in press (1997).

[11] R. H. Rangel and X. Bian, Metal-Droplet Deposition Model Including Liquid Deformation and Substrate Remelting, *Int. J. Heat Mass Transfer*, **40**, 2549-2564 (1997).

[12] Jones, H., Cooling, freezing and substrate impact of droplets formed by rotary atomization. *J. Phys. D, Appl. Phys.*, **4**, 1657-1660 (1971).

[13] Collings, E.W., Markworth, A.J., McCoy, J.K., and Saunders, J.H., Splat-Quench Solidification of Freely Falling Liquid-Metal Drops by Impact on a Planar Substrate. *J. Mater. Sc.*, **25**, 3677-3682 (1990).

[14] Chandra, S. and Avedisian, C.T., On the Collision of a Droplet With a Solid Surface. *Proceedings of the Royal Society of London, Series A*, **432**, 13-41 (1991).

[15] McPherson, R., On the Formation of Thermally Sprayed Alumina Coatings, *J. Mater. Sc.*, **15**, 3141-3149 (1980).

[16] T. Bennett and D. Poulikakos, Splat-Quench Solidification: Estimating the Maximum Spreading of a Droplet Impacting a Solid Surface, *J. Materials Science*, **28**, 963-970 (1993).

[17] Wang, G.-X., Matthys, E.F., Modelling of Heat Transfer and Solidification during Splat Cooling: Effect of Splat Thickness and Splat/Substrate Thermal Contact, *Int. J. Rapid Solidification*, **6**, 141-174 (1991).

[18] Wang, G.-X., Matthys, E.F., Numerical Modelling of Phase Change and Heat Transfer during Rapid Solidification Processes: Use of Control integrals with Element Subdivision, *Int. J. Heat Mass Transfer*, **35**, 141-153 (1992).

[19] Bennett, T. and Poulikakos, D., Heat Transfer Aspects of Splat-Quench Solidification: Modelling and Experimental, *J. Materials Sc.*, vol. 29, 2025-2039 (1994).

[20] B. Kang, J. Waldvogel, D. Poulikakos, Remelting phenomena in the Process of Splat Solidification, *J. of Materials Sc.* **30**, 4912-4925 (1995).

[21] F. P. Incropera and D. P. Witt, *Fundamentals of Heat Transfer*, P. 8. John Wiley & Sons, New York(1981).

[22] C. G. Levi, The evolution of microcrystalline structures in supercooled metal powders, *Metall. Trans. A*, **19A**, 699-708 (1988).

[23] C. G. Levi and R. Mehrabian, Heat Flow during Rapid Solidification of Undercooled Metal Droplets, *Metall. Trans. A*, **13A**, 221-234 (1982).

[24] H. S. Carslaw and J. C. Jaeger, *Conduction of Heat in Solids* , 2nd ed., p. 283, Clarendon Press, London, 1959.

[25] S. V. Patankar, *Numerical Heat Transfer and Fluid Flow* , 1st ed., pp. 52-54, McGraw Hill, New York, 1980.

Figure Captions

Fig. 1. Effect of the Stefan number and melt temperature on the solid-liquid front velocity for long times.

Fig. 2. Solid-front time evolution: effect of the substrate/melt contact resistance and undercooling.

Fig. 3. Contact-temperature time evolution: effect of the contact resistance and undercooling, (a) deposit temperature at contact plane; (b) substrate temperature at contact plane. (c) temperature jump at the contact plane.

Fig. 4. Effect of the substrate/melt contact resistance on the time evolution of the solid-front temperature.

Fig. 5. Comparison of the temperature distribution at different times: (a) solidification with undercooling; (b) solidification at thermodynamics equilibrium temperature.

Fig. 6. Effect of initial undercooling ($h = 10^6 Wm^{-2}K^{-1}$): (a) time evolution of the phase

interface; (b) time evolution of the phase interface temperature.

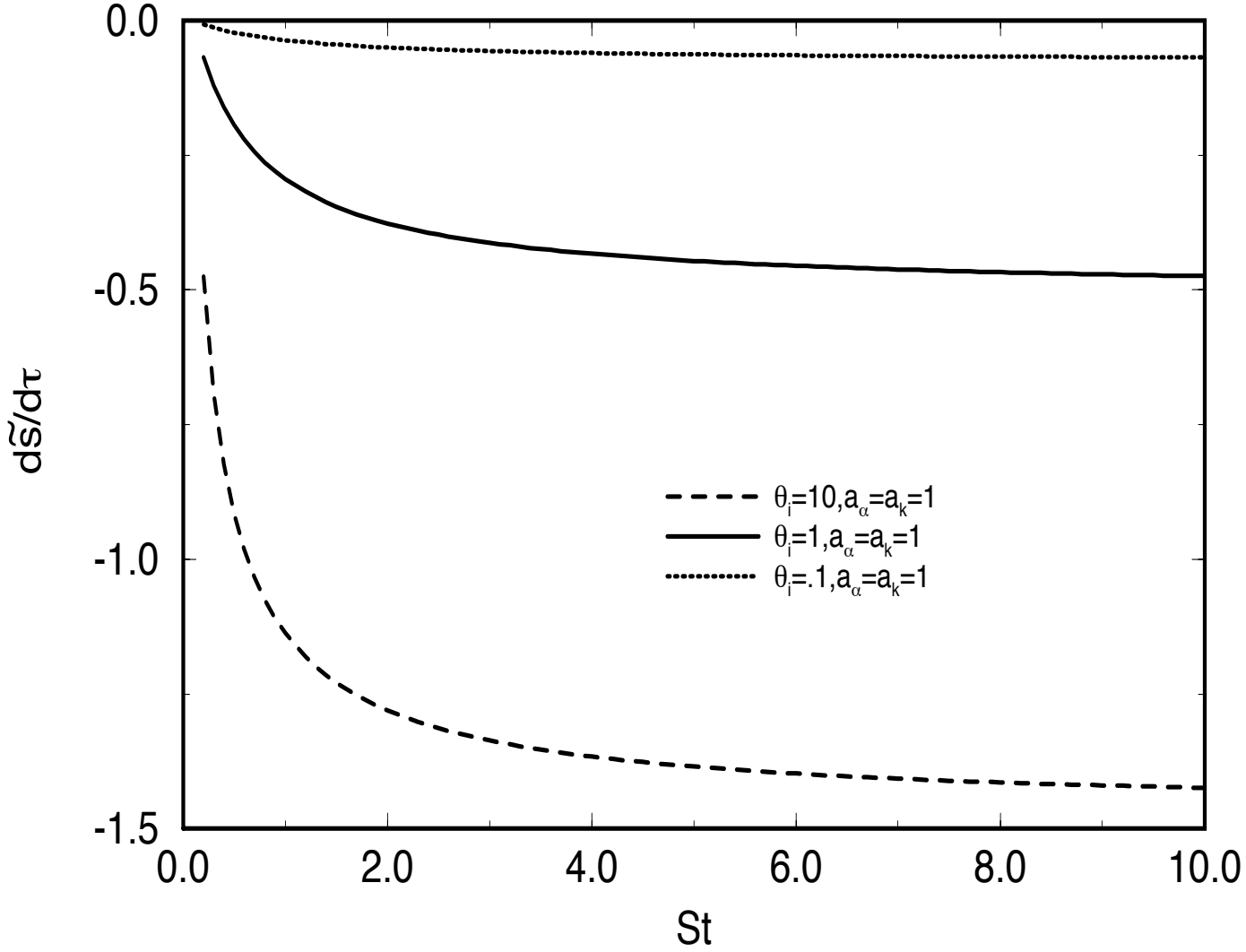

Fig. 1 Rangel and Bian

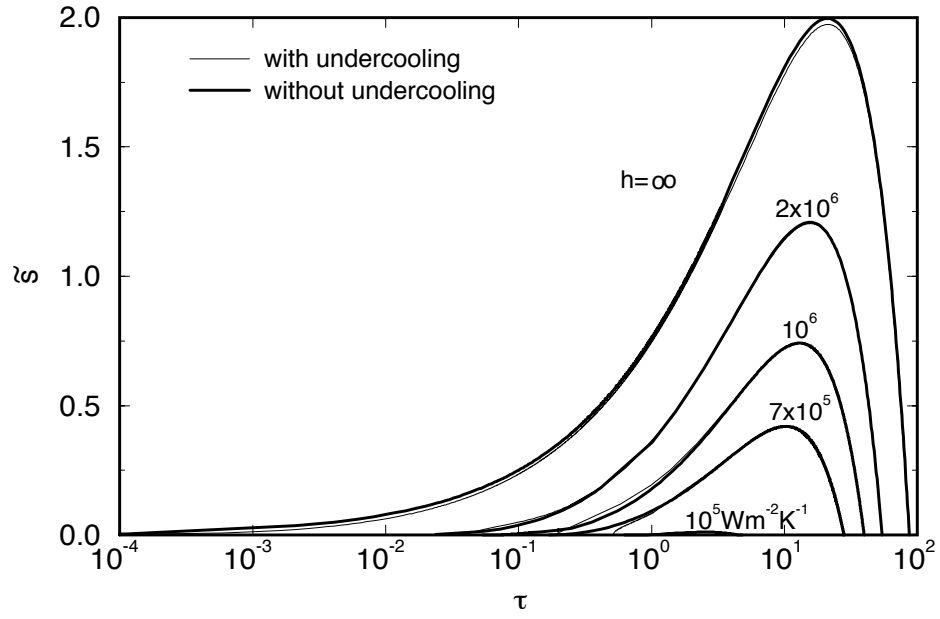

(a)

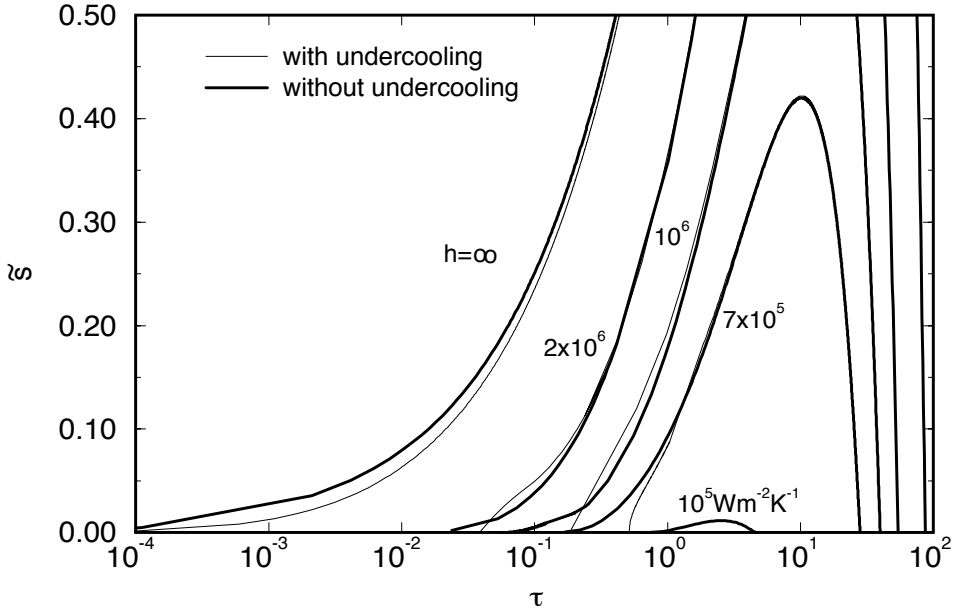

(b)

Fig. 2 Rangel and Bian

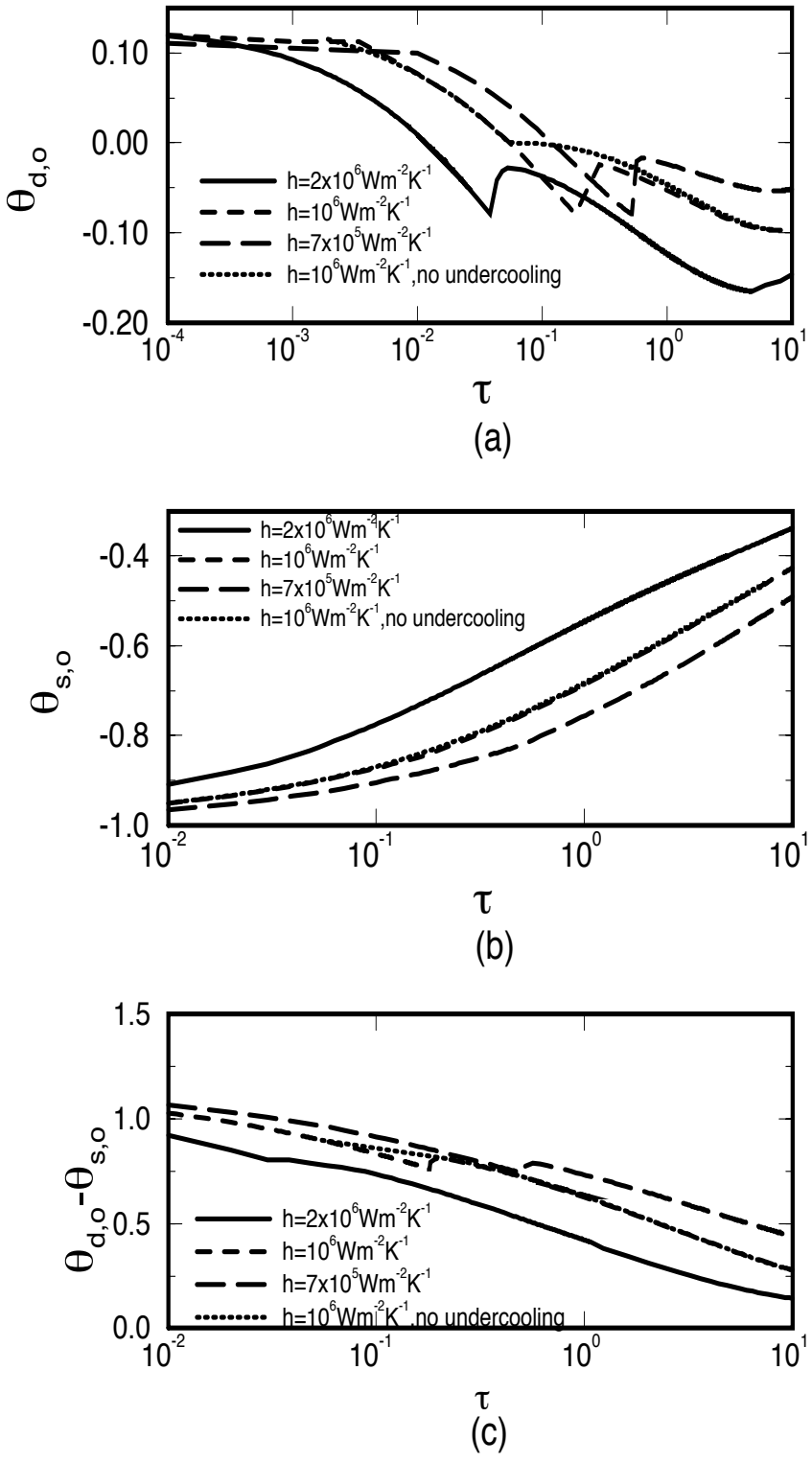

Fig. 3 Rangel and Bian

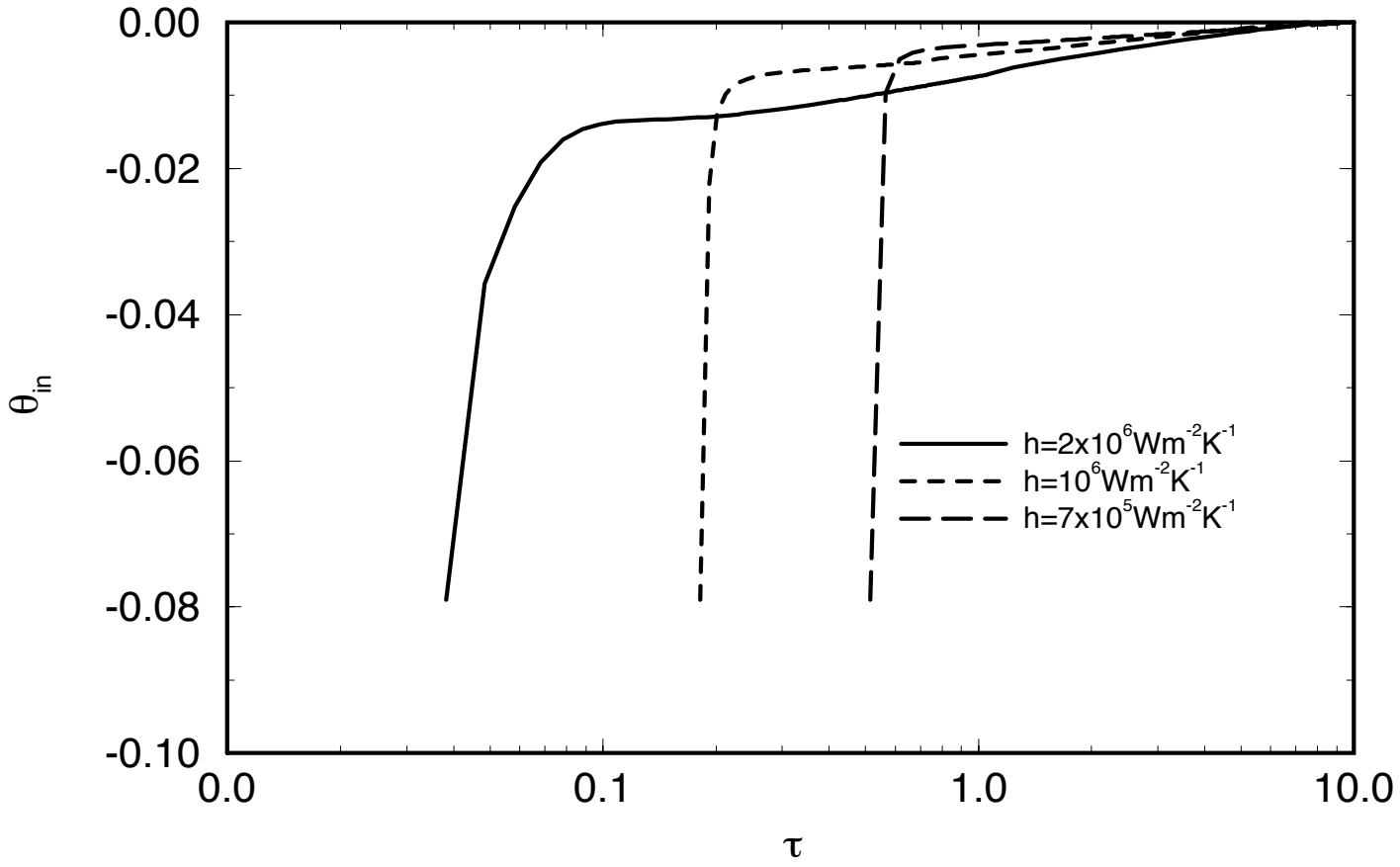

Fig. 4 Rangel and Bian

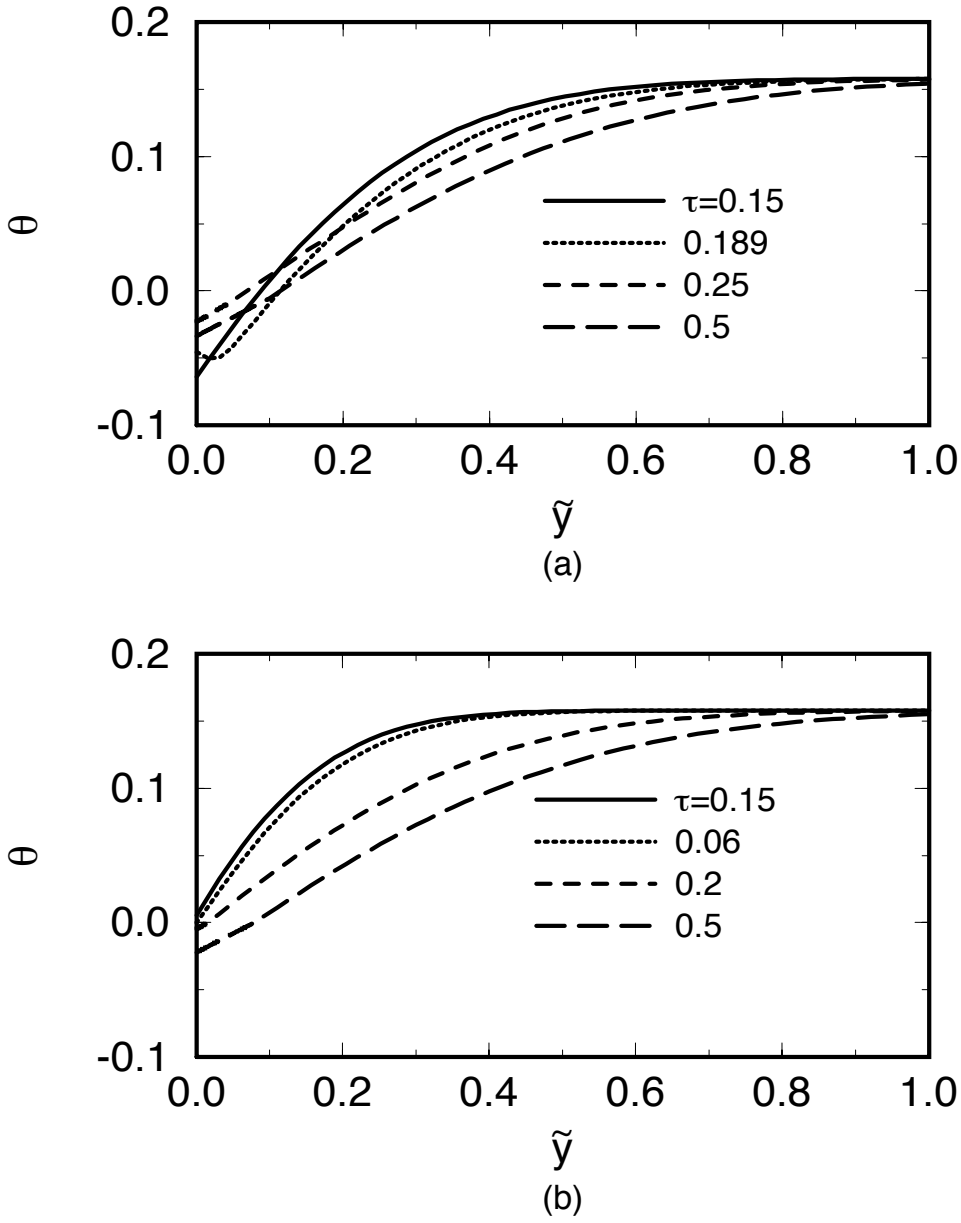

Fig. 5 Rangel and Bian

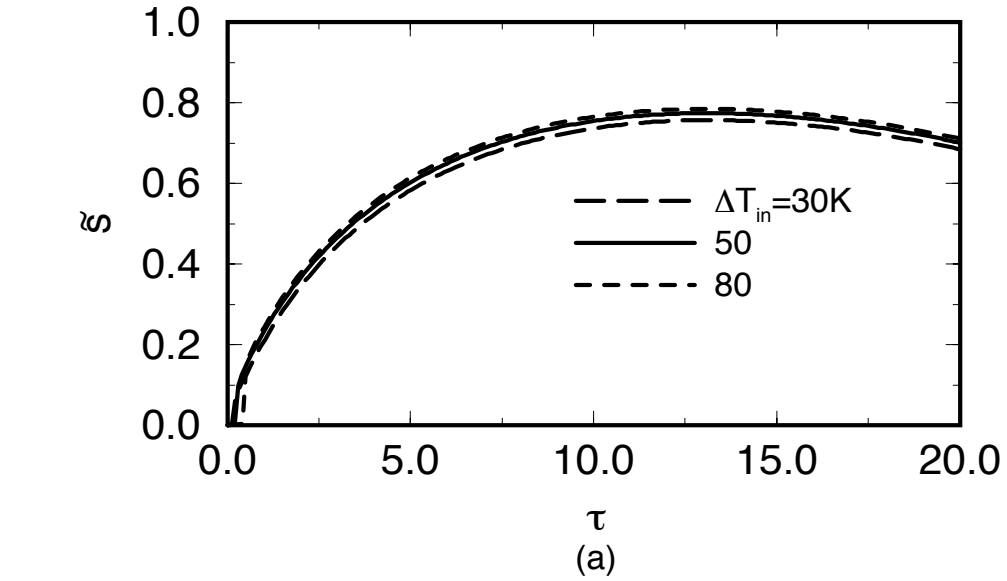

(a)

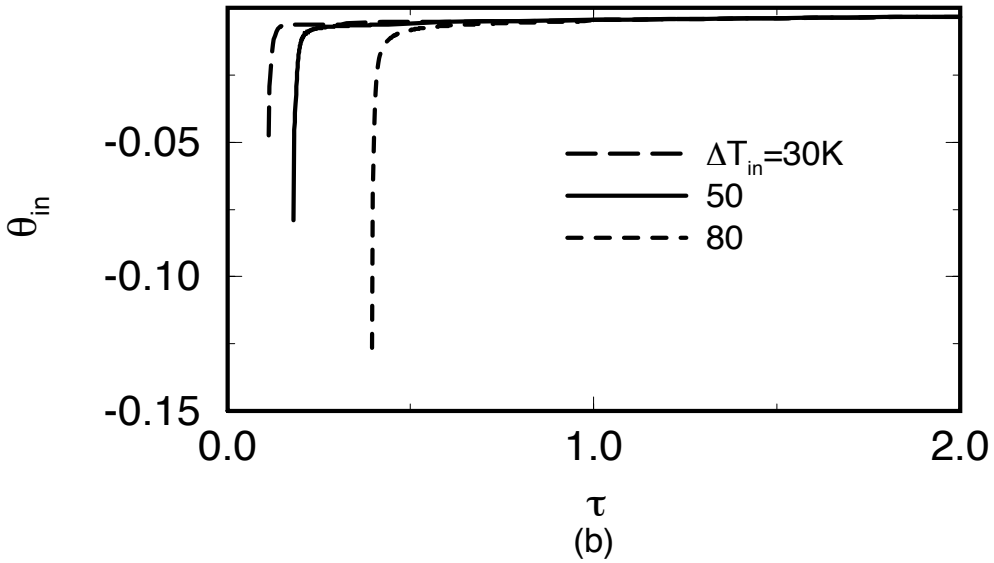

(b)

Fig. 6 Rangel and Bian